ELSEVIER

Journal of Contaminant Hydrology 54 (2002) 215–247

JOURNAL OF
Contaminant
Hydrology

www.elsevier.com/locate/jconhyd

Characterization of flow and transport processes within the unsaturated zone of Yucca Mountain, Nevada, under current and future climates

Yu-Shu Wu*, Lehua Pan, W. Zhang, G.S. Bodvarsson

Earth Sciences Division, Lawrence Berkeley National Laboratory, Berkeley, CA 94720, USA

Received 12 July 2000; accepted 30 July 2001

Abstract

This paper presents a large-scale modeling study characterizing fluid flow and tracer transport in the unsaturated zone of Yucca Mountain, Nevada, a potential repository site for storing high-level radioactive waste. The study has been conducted using a three-dimensional numerical model, which incorporates a wide variety of field data and takes into account the coupled processes of flow and transport in the highly heterogeneous, unsaturated fractured porous rock. The modeling approach is based on a dual-continuum formulation of coupled multiphase fluid and tracer transport through fractured porous rock. Various scenarios of current and future climate conditions and their effects on the unsaturated zone are evaluated to aid in the assessment of the proposed repository's system performance using different conceptual models. These models are calibrated against field-measured data. Model-predicted flow and transport processes under current and future climates are discussed.

Keywords: Unsaturated-zone flow and transport; Surface infiltration; Site characterization; Numerical simulation; Fracture–matrix interactions and perched water

1. Introduction

Characterization of unsaturated flow and transport processes in fractured rock has recently received increased attention due to their importance to underground natural resource recovery, waste storage, and environmental remediation. In the arid western United States, the thick unsaturated zone (UZ) of the highly heterogeneous, fractured

* Corresponding author. Fax: +1-510-486-5686.
E-mail address: yswu@lbl.gov (Y.-S. Wu).

0169-7722/02/$ - see front matter
PII: S0169-7722(01)00179-6

tuff at Yucca Mountain, Nevada, is currently under consideration by the US Department of Energy as a potential site for the storage of high-level radioactive waste. The UZ at Yucca Mountain, with a thickness between 500 and 700 m, has been studied extensively in the past few decades; many types of data have been collected from the site and used for characterizing the UZ system.

Quantitative investigation of water and gas flow, heat transfer, and radionuclide transport at Yucca Mountain is an essential step for conducting site-characterization studies, designing the repository and assessing the system's performance. Numerical modeling has played a crucial role in understanding the fluid movement in the unsaturated zone for evaluating the effects of hydrogeologic, thermal, and geochemical conditions on various aspects of the overall waste-disposal system. Whereas laboratory and field experiments are limited in both space and time, numerical modeling provides a means to study physical processes on large temporal and spatial scales relevant to understanding physical processes associated with nuclear waste disposal in a geologic formation. Performance-assessment models based on numerical simulation of water and gas flow, heat transfer, and tracer/radionuclide transport can include all known important physical and chemical mechanisms that affect the behavior of the potential repository and the host rock.

Characterizing the coupled processes of flow and transport in a large-scale, three-dimensional, fractured system, such as the UZ of Yucca Mountain, is both conceptually and computationally challenging. A number of numerical models for evaluating UZ hydrologic conditions at Yucca Mountain have been developed since the 1980s. Studies before the 1990s were primarily using one- and two-dimensional models to understand basic flow and transport behavior (Rulon et al., 1986; Pollock, 1986; Tsang and Pruess, 1987). In the early 1990s, Wittwer et al. (1995) started developing a three-dimensional (3-D) model that incorporated many geological and hydrological complexities, such as geological layering, degree of welding, fault offsets, different matrix and fracture properties. Ahlers et al. (1995) continued the effort of developing the UZ model with increased spatial resolution using refined grids. Their studies considered processes such as gas pressures and moisture flow, temperature and heat flow analyses, and rock property evaluation through inverse modeling. A more comprehensive mountain-scale numerical model (Wu et al., 1999a) has since been developed to study flow processes in the UZ of Yucca Mountain. A comparative study of different approaches for handling fracture and matrix flow and transport was conducted to investigate the rapid movement of solute in fractured tuffs at Yucca Mountain (McLaren et al., 2000). In parallel with flow simulation efforts, site-scale modeling studies on tracer and radionuclide transport at the site were also reported (e.g., Robinson et al., 1996; Viswanathan et al., 1998).

The site characterization in this paper has been conducted to obtain scientific understanding of flow and transport processes in the unsaturated zone of Yucca Mountain under current and future climatic conditions. In addition, the current work demonstrates how to characterize a specific site with complicated, unsaturated fracture–matrix flow and transport using a numerical model and field data. More specifically, the current effort is aimed at analyzing flow and transport behavior under various climates and different hydrogeological conceptual models. In contrast, our previous investigations (Wu et al., 1999a,b) were focused on presenting a methodology of developing and

calibrating a large, mountain-scale numerical model. The current study consists of (1) developing a new 3-D UZ flow and transport model based on the most current geological framework model and repository design; (2) assessing impacts of the nine infiltration scenarios under present-day and future climates and different perched-water conceptual models on percolation patterns; and (3) performing tracer transport studies under different flow conditions.

The primary objectives of the site characterization of this work are:

- To integrate the available data from the UZ system into a single, comprehensive, and calibrated 3-D model for simulating the ambient hydrological and geochemical conditions for use in predicting system response to future climate conditions
- To quantify the moisture flow through the UZ, under present-day and estimated future climate scenarios
- To estimate radionuclide transport times

The following issues are considered critical to the performance of the potential repository:

- The spatially and temporally averaged values of the percolation flux at the potential repository horizon
- The components of fracture and matrix flow and interactions within and below the potential repository horizon
- The effects of observed perched-water zones, and associated flow barriers and lateral flow diversion
- The probable flow paths from the potential repository to the water table
- The effects of faults on UZ flow and transport processes
- The role played by the Paintbrush nonwelded (PTn) unit in lateral flow diversion and damping infiltration pulse
- The tracer transport times, potential radionuclide migration paths from the potential repository to the water table and breakthrough curves and collection areas at the water table.

To achieve the above objectives, we have calibrated the UZ model using available field data, including field-observed matrix saturation, water potential, and perched-water data. A series of model calibrations and sensitivity analyses have then been conducted with the 3-D model to investigate the effects of variations in rock and fault properties and in model boundary conditions, using different perched-water conceptual models as well as different climate conditions.

This work is divided into the two categories: UZ flow analysis and UZ tracer transport analysis. The UZ flow characterization covers the areas of percolation fluxes, steady–steady flow fields, fracture–matrix flow components, lateral flow diversion, perched-water zones, and the effects of major faults and geological units. The tracer transport analysis focuses on estimates of tracer transport times and pathways from the repository level to the water table.

2. UZ model description

2.1. Geological model and numerical grid

The area domain of the UZ model encompasses approximately 40 km^2 of Yucca Mountain (Fig. 1). The UZ is between 500- and 700-m thick, overlying a relatively flat water table in the vicinity of the potential repository area. The proposed repository would be located in the highly fractured Topopah Spring Welded unit, more than 200 m above the water table. Yucca Mountain is a structurally complex system of Tertiary volcanic rock. Subsurface hydrologic processes in the UZ occur in a heterogeneous environment of layered, anisotropic, fractured volcanic rocks (Scott and Bonk, 1984), consisting of alternating layers of welded and nonwelded ash flow and air fall tuffs.

The primary geologic formations found at Yucca Mountain, beginning from the land surface, consist of the Tiva Canyon, Yucca Mountain, Pah Canyon, and the Topopah Spring Tuffs of the Paintbrush Group. Underlying these are the Calico Hills Formation,

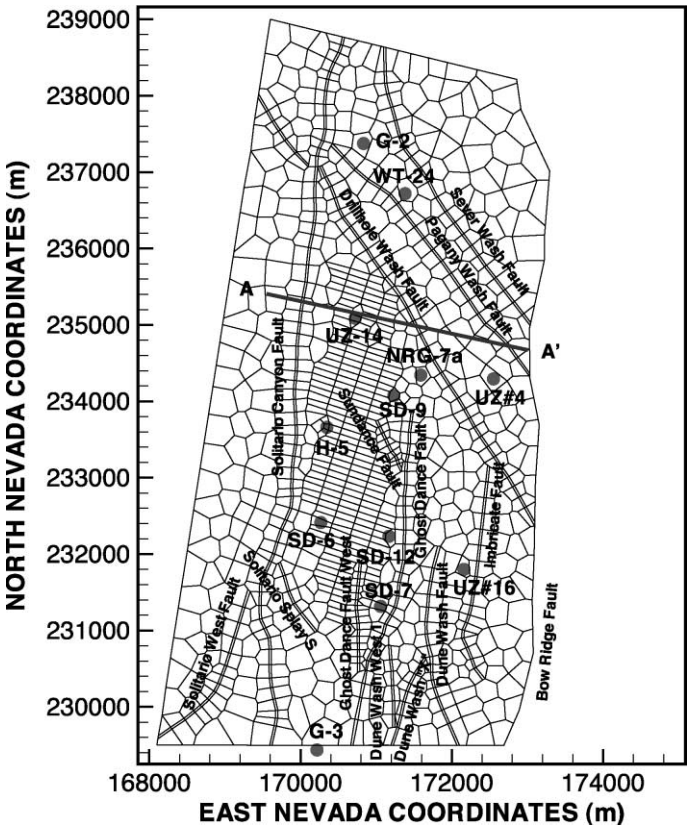

Fig. 1. Plan view of the 3-D UZ model grid, showing the model domain, faults incorporated and borehole locations at the Yucca Mountain.

and the Prow Pass, Bullfrog, and Tram Tuffs of the Crater Flat Group (Buesch et al., 1995). These geologic formations have been reorganized into hydrogeologic units based primarily on the degree of welding (Montazer and Wilson, 1984). These are the Tiva Canyon welded (TCw) hydrogeologic unit, the Paintbrush nonwelded unit (PTn), consisting primarily of the Yucca Mountain and Pah Canyon members and their bedded tuffs, the Topopah Spring welded (TSw) unit, the Calico Hills nonwelded (CHn), and the Crater Flat undifferentiated (CFu) units. The hydrogeological units vary significantly in thickness over the model domain.

An essential requirement of a valid 3-D grid for representing the UZ system is to preserve the important geological characters, such as layers and faults, which have significant impact on flow and transport modeling results. The 3-D, irregular, control-volume grid (Fig. 1) is generated using the WinGridder mesh generator (Pan et al., 2000). Fig. 1 shows a plan view of the resulting 3-D model grid as well as the horizontal model domain. Note that the 3-D UZ grid uses relatively refined meshes in the vicinity of the proposed repository, located near the center of the model domain. Also shown in Fig. 1 are the locations of several boreholes, used in model calibrations and analyses. Each gridblock in the plan ($x-y$) plane on Fig. 1 represents a vertical column in the 3-D grid. Shown in Fig. 2 is a vertical cross section of the 3-D grid, displaying grid layers, geological units (using code-letter names), faults, and the potential repository location along the west–east section (A–A′) of Fig. 1.

In addition to the highly heterogeneous nature of the fractured tuffs at the mountain, flow and transport processes are further complicated by numerous strike-slip and normal faults with varying amounts of offset (Scott and Bonk, 1984; Day et al., 1998). The vertical offset along these faults commonly ranges from ten to hundreds of meters, and generally increases from north to south. These major faults generally penetrate the

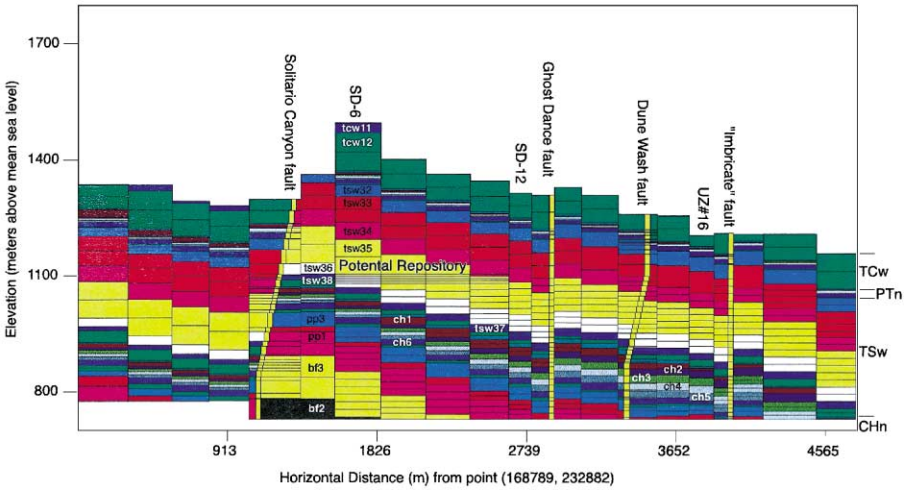

Fig. 2. Cross-section grids through the 3-D model, showing the vertical gridding and offsets of the explicitly modeled faults along the west–east cross section (A–A′ of Fig. 1).

complete UZ thickness. Faults are important to be included in the UZ model grid since they may provide fast pathways for flow and transport or serve as barriers to lateral flow. Conceptually, three important features of a fault are conserved in the numerical grid. First, a fault serves as a separator that causes discontinuity of geological layers and may serve as a structural barrier to lateral flow under unsaturated conditions. Second, a fault zone is continuous and may serve as a fast path for downward flow. Third, a fault may not be vertical, and its angle of inclination may vary spatially. Implementation of these fault features in the UZ grid is shown in Figs. 1 and 2.

The 3-D UZ model grid, as shown in Figs. 1 and 2, has 1324 mesh columns of both fracture and matrix continua and 37 computational grid layers in the vertical direction, resulting in 97,976 gridblocks and 396,770 connections in a dual-permeability grid.

2.2. Modeling approaches

The simulation results presented in this study were obtained using the TOUGH2 and T2R3D codes (Pruess, 1991; Wu et al., 1996). The conservation equations involve mass of air, water, and chemical components as well as thermal energy are discretized using the integral finite-difference method. The discretization method makes it possible, by means of simple preprocessing of geometric data, to implement double- and multiple-porosity, or dual-permeability methods for treatment of flow and transport in fractured porous media. The TOUGH2 formulation handles the time fully implicitly, using a first-order backward finite-difference scheme. The resulting discretized finite difference equations for mass and energy balances are nonlinear and are solved using the Newton/Raphson iterative scheme.

Fracture–matrix interactions in this work are handled using the dual-permeability model. This method has a better handling of transient flow and transport than the effective continuum method and computationally much less demanding than the discrete-fracture-modeling approach. Both matrix–matrix flow and fracture–fracture flow are considered important to moisture movement in the UZ of Yucca Mountain (Robinson et al., 1996) such that the dual-permeability approach has become the main approach used in the modeling studies of Yucca Mountain Project (Wu et al., 1999a,b). The dual-permeability methodology considers global flow and transport occurring not only between fractures but also between matrix grid blocks. In this approach, the domain is represented by two overlapping (yet interacted) fracture and matrix continua and fracture–matrix flow is approximated as quasi-steady (Warren and Root, 1963). As applied in this study, the traditional dual-permeability concept is further modified using an active fracture model (Liu et al., 1998) to represent fingering flow effects through fractures.

2.3. Model boundary conditions

The ground surface of the mountain is taken as the top 3-D model boundary, and the water table is treated to be spatially fixed as the bottom boundary. For flow simulations, surface net infiltration is applied to the top boundary using a source term. The bottom boundary, the water table, is treated as a Dirichlet-type boundary. All the lateral

boundaries, as shown in Figs. 1 and 2, are treated as no-flow (laterally closed) boundaries. This is reasonable because these lateral boundaries are either far away or separated from the repository by faults, and no-flow boundaries should have little effect on moisture flow and tracer transport within or near the potential repository area.

2.4. Current and future climates

Current and possible future climates are implemented into the model in terms of net surface infiltration rates in the modeling studies. Net infiltration of water resulting from precipitation is the most important factor affecting the overall hydrological, geochemical and thermal–hydrologic behavior of the UZ. Infiltration and percolation through the UZ provide a vehicle for transporting radionuclides from the repository to the water table. In an effort to cover various possible scenarios and uncertainties of future, a total of nine net infiltration maps are implemented into the modeling studies. These infiltration rates are estimated by the US Geological Survey (USGS) scientists (Hevesi and Flint, 2000; Forrester, 2000) for the site. The nine infiltration maps represent present-day, monsoon, and glacial transition—three climatic scenarios. Each of the three scenarios is represented by lower-bound, mean, and upper-bond values.

The statistics of the nine infiltration rates are summarized in Table 1 for average values over the model domain. The lower- and upper-bound infiltration values for each climate scenario are intended to cover the uncertainties of possible higher or lower ranges of rates. The two future climatic scenarios (i.e., the monsoon and glacial transition periods) are used to account for possible higher precipitation and infiltration conditions in the future climates at the mountain. A plan view of the spatial distributions for the nine infiltration maps, as interpolated onto the model grid, is shown in Fig. 3(a)–(i), respectively, for the present-day, monsoon and glacial transition infiltration scenarios of lower-, mean and upper-bounds. The figures show similar distribution patterns, but very different values with the nine maps, and higher recharge rates are located in the northern part of the model domain and along the mountain ridge from south to north. Net infiltration pattern at Yucca Mountain is spatially highly variable because of variations in soil cover and precipitation (Flint et al., 1996). Although substantial research efforts have been devoted to determination of net infiltration over the mountain, direct measurements were proven difficult due to the low moisture flux and high potential evapotranspiration rates at the mountain area. Net infiltration rates (Fig. 3) have been estimated based on average annual precipitation and other field observation data using a modeling method (Hevesi and Flint, 2000).

Table 1
Average values of infiltration rates over the UZ model domain

Climate scenario	Lower infiltration (mm/year)	Mean infiltration (mm/year)	Upper infiltration (mm/year)
Present-day	1.20	4.56	11.24
Monsoon	4.60	12.36	20.12
Glacial transition	2.40	17.96	33.52

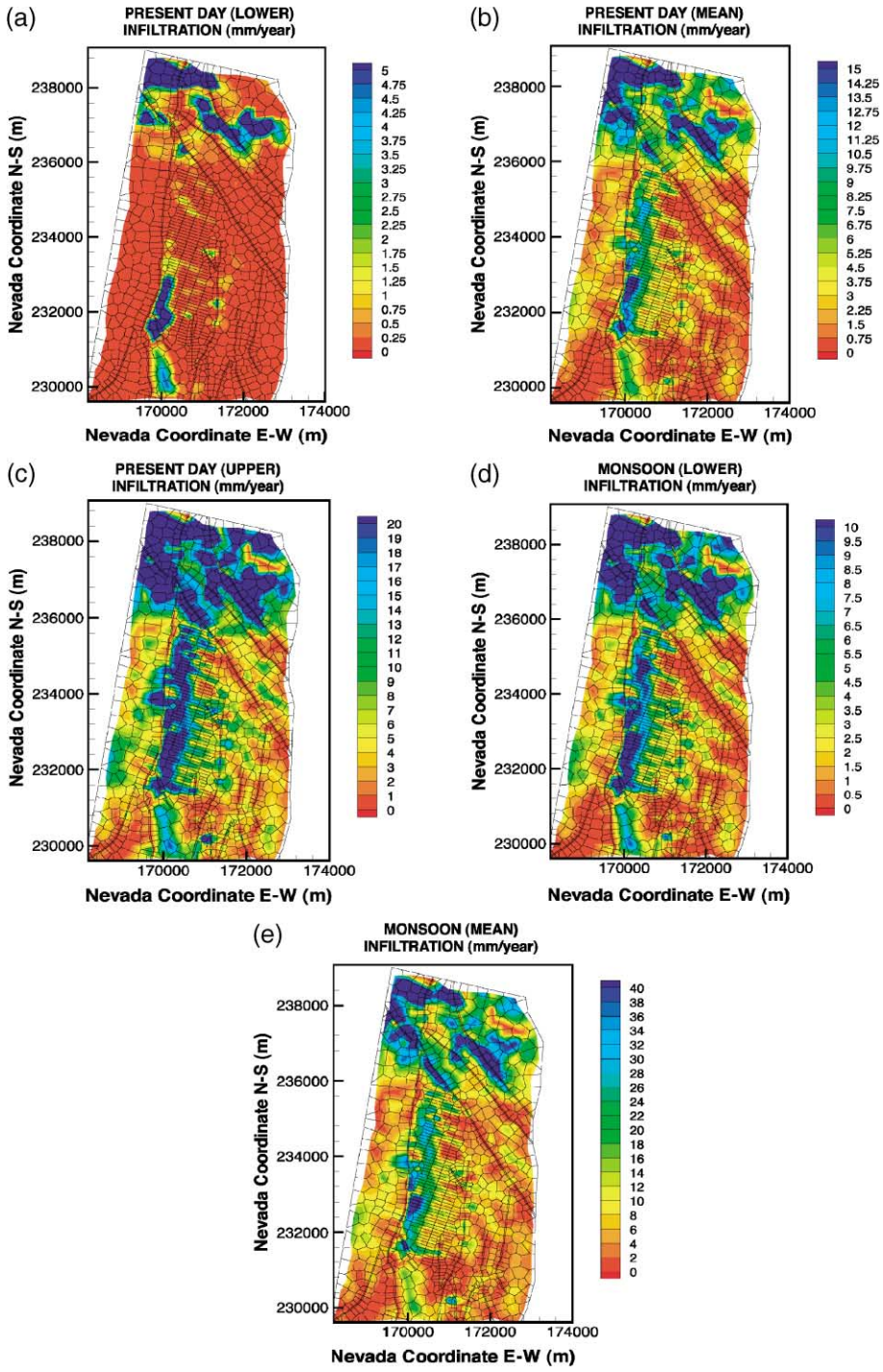
(a)
PRESENT DAY (LOWER)
INFILTRATION (mm/year)
(b)
PRESENT DAY (MEAN)
INFILTRATION (mm/year)
(c)
PRESENT DAY (UPPER)
INFILTRATION (mm/year)
(d)
MONSOON (LOWER)
INFILTRATION (mm/year)
(e)
MONSOON (MEAN)
INFILTRATION (mm/year)
Nevada Coordinate N-S (m)
Nevada Coordinate E-W (m)
238000
236000
234000
232000
230000
170000
172000
174000

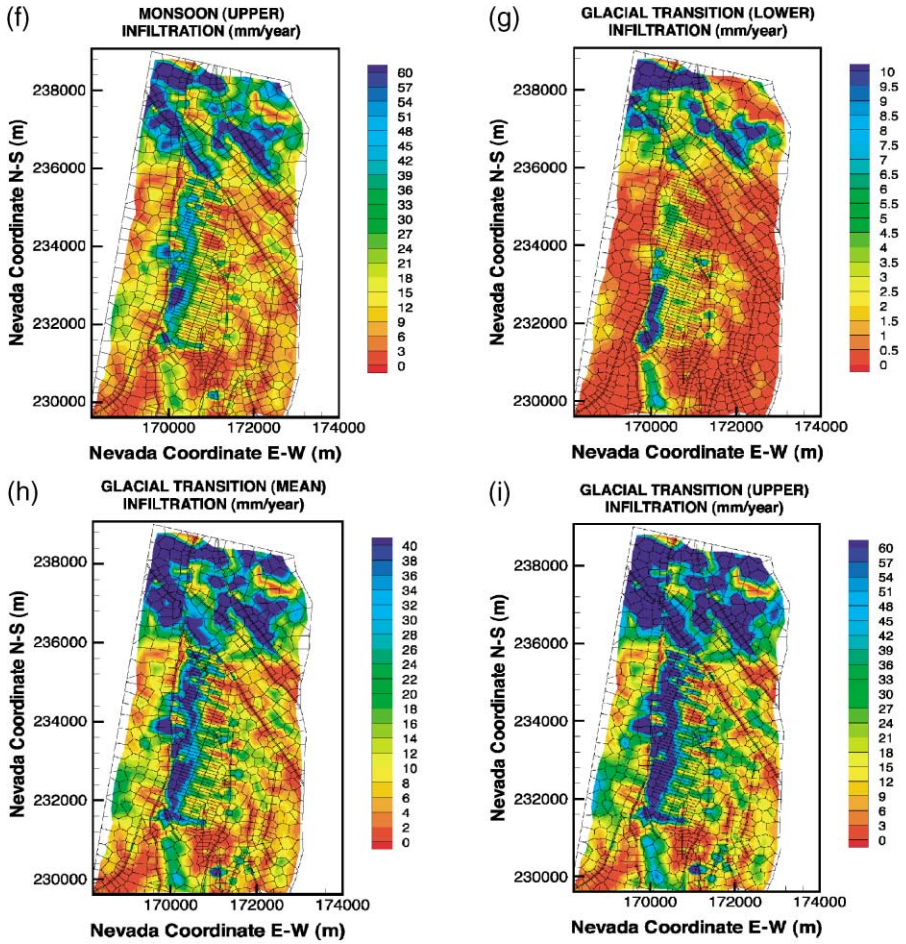

Fig. 3. Net infiltration maps for the nine current and future climate scenarios, (a) present-day, lower-bound; (b) present-day, mean; (c) present-day, upper-bound; (d) monsoon, lower-bound; (e) monsoon, mean; (f) monsoon, upper-bound; (g) glacial, lower-bound; (h) glacial, mean; and (i) glacial, upper-bound.

2.5. Model parameters and rock properties

The input parameters for rock and fluid properties include (1) fracture properties [frequency, permeability, van Genuchten (1980) α and m parameters, aperture, porosity, and interface area], (2) matrix properties (porosity, permeability, and the van Genuchten α and m parameters), and (3) transport properties (grain density, tortuosity, diffusion, decay and sorption coefficients), respectively, for each model layer. Fault properties (matrix and fracture parameters) are also needed for each unit of TCw, PTn, TSw and CHn. The development of these parameters is presented in several related studies (Ahlers and Liu, 2000; Liu, 2000), and calibration of 3-D model properties is discussed below. These estimated rock and fluid properties (Wu et al., 2000) are used in the present study.

Based on the geological conceptual model, the rock parameters are estimated and specified in general layer by layer in the model, although certain areas in the CHn unit are altered to vitric or zeolitic regions. In these property-altered layers, zeolitic and vitric tuff properties are specified to correspond to actual geologic properties according to the alteration layers. We treat all of the geological units, including fault zones, as fracture–matrix systems using the dual-permeability concept. The van Genuchten relative permeability and capillary pressure functions (van Genuchten, 1980) are used to describe variably saturated flow in both fracture and matrix media.

3. Model calibration with moisture and perched-water data

Model calibration is a critical step in developing a representative model of the UZ system of Yucca Mountain. In model calibration studies, field-measured liquid saturation, water potential, pneumatic, and perched-water data are used to estimate input parameters of the 3-D model. The model calibration efforts in this work are focused on matching perched-water occurrences using a 3-D model (though they also match matrix liquid saturation and water-potential data, as well). During field investigations, several perched water zones were encountered in the UZ of the site (Rousseau et al., 1998; Wu et al., 1999b), including UZ-14, SD-7, SD-9, SD-12, NRG-7a, G-2, and WT-24 (see Fig. 1 for their locations). These perched-water occurrences were found mostly to be associated with low-permeability zeolites in the CHn or the densely welded basal vitrophyre of the TSw unit.

The presence of perched-water bodies in the vicinity of the potential repository at Yucca Mountain has a potential impact on the repository performance, and at the same time it provides invaluable insight into water movement, flow pathways, and the surface infiltration history of the mountain. For example, it implies that water may not travel vertically through the unsaturated zone to the water table directly, but has somehow been trapped or diverted laterally. As a result, perched-water zones may divert water around low-permeability zeolitic layers that have substantial capacity to retard radionuclide transport by sorption.

A permeability-barrier conceptual model for perched-water occurrence has been used in the UZ flow modeling studies since 1996, as summarized in Wu et al. (1999b). The major assumptions with the permeability-barrier concept (Conceptual Model #1) of this study are: (1) no large-scale vertically connected fractures transect the underlying low-permeability units, (2) both vertical and horizontal permeabilities within and below the perched-water zone are small compared with permeabilities outside perching zones, and (3) sufficient percolation flux (>1 mm/year) exists.

A second model (Conceptual Model #2) is an unfractured zeolite model. Similar to the permeability barrier Model #1, this model presumes that the occurrence of perched water at Yucca Mountain results mainly from the lack of globally connected fractures within zeolitic units. This model can be considered a special case of the permeability barrier model, in which a water-perching mechanism is controlled by the low-permeability zeolitic matrix only (i.e., the effects of fractures on flow in zeolites in the entire CHn unit are ignored). The concept of an unfractured zeolite model is partially supported by the observed fracture data (Liu, 2000), which suggest a very small fracture frequency within zeolitic units.

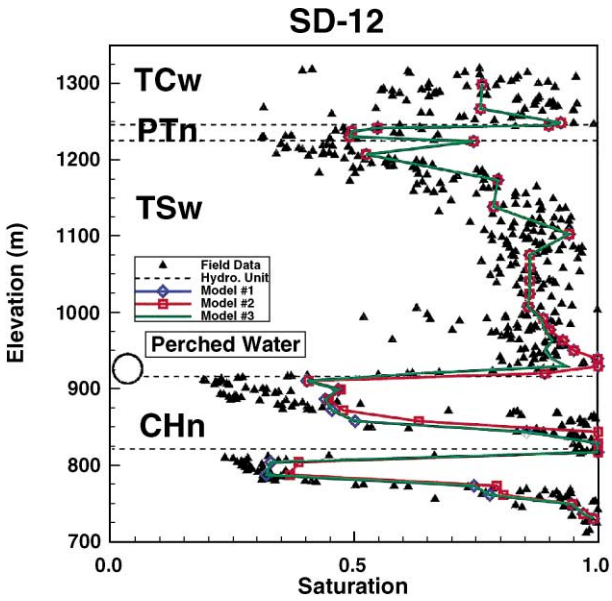

Fig. 4. Comparison of simulated and observed matrix liquid saturations and perched-water elevations for borehole SD-12, using the three conceptual models with present-day, mean infiltration rate (with the thin-dashed lines representing interfaces between hydrogeological units).

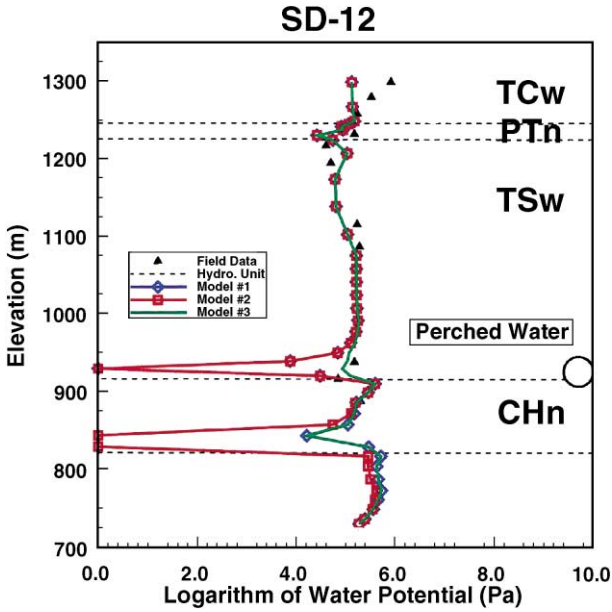

Fig. 5. Comparison of simulated and observed water potential and perched-water elevations for borehole SD-12, using the three conceptual models with present-day, mean infiltration rate (with the thin-dashed lines representing interfaces between hydrogeological units).

In the present numerical studies, the occurrence of perched water is assumed to follow either of the two conceptual models, permeability-barrier model or unfractured zeolite model. In other words, a perched-water body is formed mainly as a result of permeability-barrier effects. Conceptual Model #3 under consideration is a nonwater-perching model. This model is introduced mainly for sensitivity analyses and comparative studies with the two water-perching models.

To calibrate the 3-D model against observed perched-water conditions at Yucca Mountain, some local modification of rock properties is necessary. For Conceptual Model #1, calibrated parameters of fracture and matrix permeabilities within perched zones were manually calibrated from a series of 3-D modeling studies. Matrix permeabilities of potential perched layers/zones are based on average values of the measured matrix permeabilities, while fracture permeabilities used for the northern perched zones are assumed to be 10 times higher than matrix permeabilities. Other than intrinsic permeabilities, van Genuchten's α and m parameters, as well as residual saturations for matrix blocks within perched zones, are identical to parameters estimated from the inverse modeling studies using moisture, pneumatic and geochemical data (Ahlers and Liu, 2000). For Conceptual Model #2, the unfractured zeolite model, rock properties of all the fractures within the potential perched layers/zones are replaced by the corresponding matrix properties from the inversion (Ahlers and Liu, 2000). There are a total of seven sets of properties used in this study, for different infiltration rates and perched-water conceptual models (Wu et al., 2000).

In the following, the simulation results are presented and discussed in terms of (1) comparisons with matrix liquid saturation and water potential data, and (2) match with observed perched-water bodies. We have checked all simulation results with the two perched-water conceptual models against observed saturation, water potential, and perched-water data at all the observation boreholes. For brevity, Borehole SD-12 is selected to show the match between observed and modeled vertical-saturation, water potential profiles and perched-water locations (Figs. 4 and 5), respectively. In general, the modeled results from all the simulations are in reasonable agreement with the measured saturation data (Fig. 4) and with measured water potential profiles (Fig. 5). Note that below the top of the CHn unit, no measured water potential data for SD-12 are available for comparison. In addition, the observed perched-water elevation and water potential data at the perched level seem to be contradicted to each other, because the water potential at perched-water zones should be (near) zero, which is not shown by the field data (Fig. 5) and needs further studies.

Also shown in Figs. 4 and 5 are the water-perching elevations at this borehole, indicating a good agreement between what was observed and what was simulated using the two perched-water conceptual models. The nonwater-perching model (Conceptual Model #3) cannot predict perched-water conditions in the borehole.

4. Flow patterns and analyses

The UZ flow modeling studies discussed in this section are conducted for insights into flow behavior within the UZ system. These studies are based on the results from 21 3-D

steady-state flow simulations under different perched-water conceptual models and climate scenarios. This section summarizes the modeling results, including modeled percolation fluxes and flow fields, fracture and matrix flow components, and specific studies of PTn and CHn hydrogeological units, perched-water occurrence, and major fault effects.

4.1. Percolation flux at the potential repository horizon

Percolation flux through the UZ is one of the most critical factors affecting potential repository performance. The quantity and spatial and temporal variations in percolation flux directly affect: (1) the amount of water flowing into waste emplacement drifts; (2) moisture conditions and the corrosion environment of canisters within the drifts; (3) waste mobilization from the potential repository; (4) thermo-hydrologic behavior of the potential repository; and (5) radionuclide migration from the UZ to the saturated zone. However, because percolation fluxes of unsaturated flow cannot be readily measured in the field, we must rely on indirect data and model results to estimate these for total system performance assessment (TSPA) of the Yucca Mountain site.

The past modeling studies (Wu et al., 1999a,b) indicate that accurate model predictions of percolation fluxes at Yucca Mountain depend on many factors. The most important ones are: (1) net infiltration rates over the surface boundary under various climate scenarios; (2) representative geological and conceptual models; (3) reliable distributed rock property values for fractures and matrix blocks; and (4) treatment of fracture–matrix flow and interactions. Percolation fluxes at the repository horizon, as predicted by the current model, have been analyzed using 21 3-D UZ flow simulation results, with nine infiltration maps, representing current and future climates, and the three conceptual models.

Fig. 6(a)–(i) shows samples of percolation fluxes simulated at the repository level for the nine infiltration rates of present-day, monsoon and glacial-transition climates. As discussed for the perched-water studies, differences in perched-water models are only reflected in fracture–matrix properties in the CHn, which have little effect on the upstream flow above the CHn unit, such as at the higher-elevation repository level. Modeling results show that simulated percolation fluxes at the potential repository are similar to the surface infiltration flux (Fig. 3).

Fig. 6 displays a highly nonuniform pattern of flux distributions (the darker blue spots on the figure indicates the higher percolation fluxes modeled). In this figure, the percolation flux is defined as total vertical liquid mass flux per year through both fractures and matrix in mm/year, which is the commonly used unit for surface infiltration. The high percolation fluxes are located primarily at the northern part, secondarily along the Solitario Canyon fault and the crest in the middle portion of the model domain. A similarity between the modeled percolation fluxes at repository level and their corresponding surface infiltration values (Fig. 3) indicates that no large-scale lateral flow diversion occurs when flowing from surface to repository level. Beneath the repository horizon, as discussed below, the distribution of percolation fluxes is more diffuse and generally spread to the east as a function of lateral flow.

The statistics of the averaged percolation fluxes within the repository footprint, extracted from the 3-D flow model results for the three mean infiltration scenarios, are listed in Table 2. The table indicates that the total percolation flux within the potential

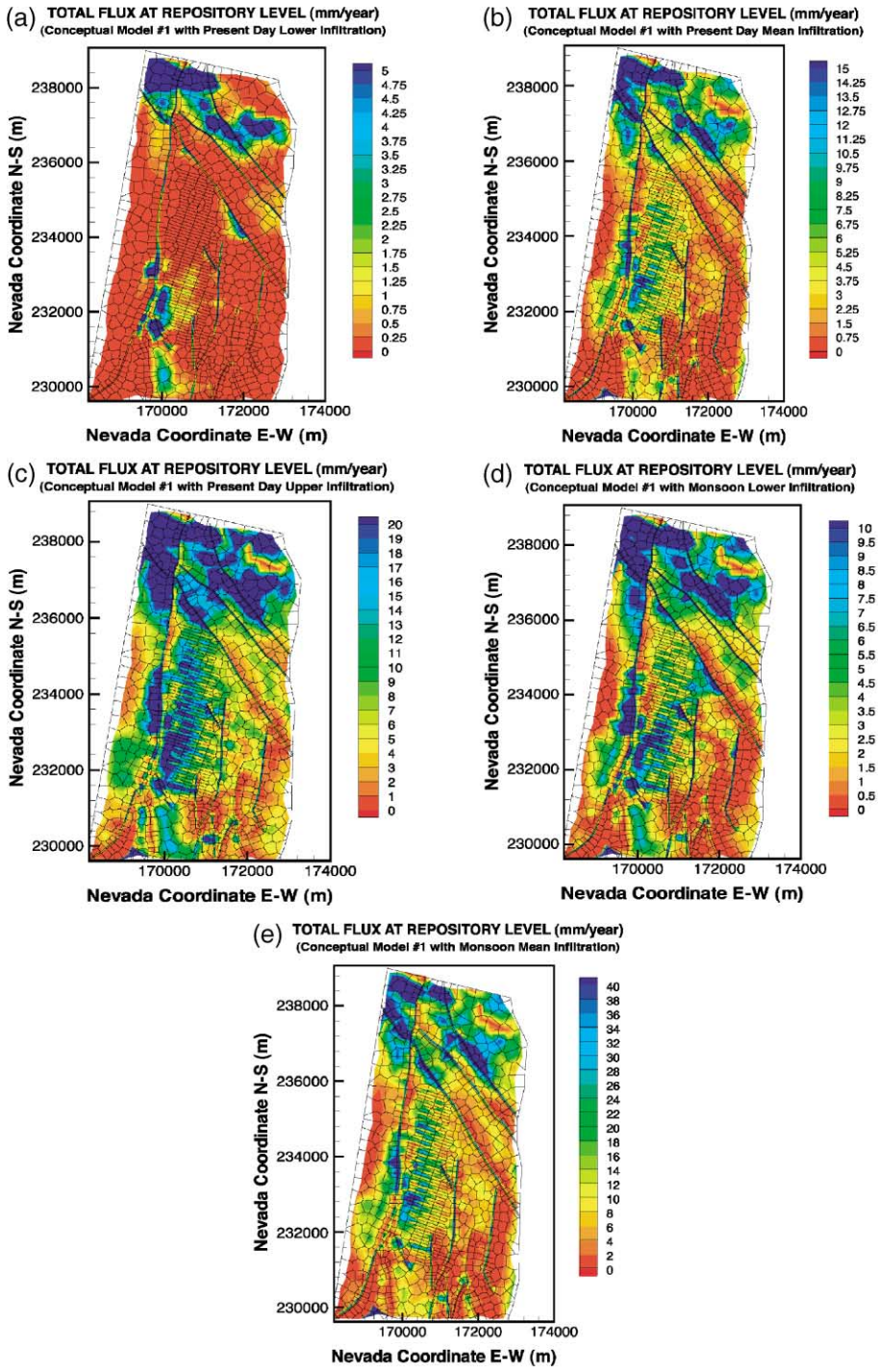
(a) TOTAL FLUX AT REPOSITORY LEVEL (mm/year)
(Conceptual Model #1 with Present Day Lower Infiltration)
(b) TOTAL FLUX AT REPOSITORY LEVEL (mm/year)
(Conceptual Model #1 with Present Day Mean Infiltration)
(c) TOTAL FLUX AT REPOSITORY LEVEL (mm/year)
(Conceptual Model #1 with Present Day Upper Infiltration)
(d) TOTAL FLUX AT REPOSITORY LEVEL (mm/year)
(Conceptual Model #1 with Monsoon Lower Infiltration)
(e) TOTAL FLUX AT REPOSITORY LEVEL (mm/year)
(Conceptual Model #1 with Monsoon Mean Infiltration)
Nevada Coordinate N-S (m)
Nevada Coordinate E-W (m)
238000
236000
234000
232000
230000
170000
172000
174000

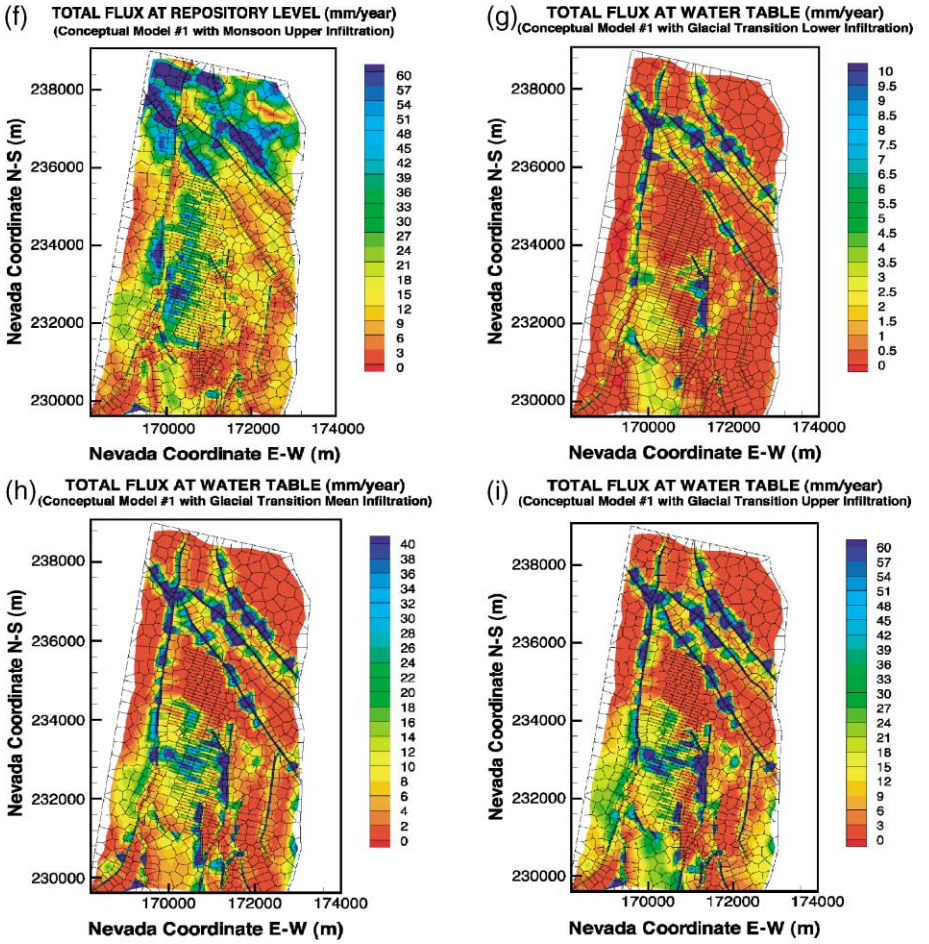

Fig. 6. Simulated fluxes at repository using Conceptual Model #1, for the nine current and future climate scenarios: (a) present-day, lower-bound; (b) present-day, mean; (c) present-day, upper-bound; (d) monsoon, lower-bound; (e) monsoon, mean; (f) monsoon, upper-bound; (g) glacial, lower-bound; (h) glacial, mean; and (i) glacial, upper-bound.

repository is very similar to the average surface infiltration rate over the entire model domain of Table 1. The only exception is the glacial-transition scenario, which predicts a higher average percolation flux within the repository footprint than the average value over the entire model domain.

Percolation fluxes within the repository footprint can be further analyzed using a frequency distribution plot, which displays the average percentage of the repository area subject to a particular percolation rate. This information is important to drift-scale modeling studies of flow and transport at drifts and flow focusing phenomena through the TSw. Fig. 7 shows the frequency distribution of normalized percolation flux within the repository horizon for the three mean infiltration rates.

Table 2
Average percolation fluxes simulated within the potential repository footprint for the three mean infiltration scenarios

Climate scenario; mean infiltration over the UZ model domain (mm/year)	Average percolation flux within potential repository (mm/year)		
	Fracture	Matrix	Total
Present-day; 4.6	4.02	0.52	4.54
Monsoon; 12.4	12.11	0.79	12.90
Glacial transition; 18.0	19.52	0.94	20.46

Fig. 7(a) indicates that the highest flux frequencies have fluxes within the 1.0–4.0 mm/year range and occur over about 50% of the repository area. The nodal area with percolation fluxes greater than 20.0 mm/year comprises only about 1% of the total repository area. For the monsoon scenario, Fig. 7(b) shows that the highest frequency of percolation fluxes is in a range of about 6 to 7 mm/year, occurring over 18% of the total repository area. Less than 1% of the repository area is subject to 50 mm/year or higher percolation rates. For the high-infiltration, the glacial-transition climate, the highest areal frequency of percolation fluxes is in the range of 8 to 13 mm/year (Fig. 7(c)), 25% of the total repository area, and less than 3% of the repository area is subject to 60 mm/year or higher percolation flux. In general, the percolation flux value with highest areal frequencies is lower than the average values of the corresponding infiltration rates.

4.2. Fracture and matrix flow components

Steady-state fracture and matrix flow components can also be analyzed using the UZ flow model results. This analysis examines the effect of various climate scenarios and perched-water conceptual models on fracture and matrix flow, especially at the repository level of the TSw unit. Fracture flow is expected to dominate percolation where flux exceeds the hydraulic conductivity of the matrix. This is most likely to occur within the densely welded units, such as in the TSw. Fracture flow has important implications for flow into emplacement drifts and therefore may directly impact the long-term performance of the potential repository. In addition, fractures provide preferential fast flow paths from the ground surface to the repository level and from the repository level to the water table. For these reasons, the conceptual model of fracture flow is of major concern for calculations of radionuclide releases from the potential repository.

Similar to percolation fluxes, fracture and matrix flow components are difficult to measure directly at the site. The partitioning of flow between fractures and matrix must, therefore, be inferred from modeling results. Examples of simulated fracture and matrix flow at the repository horizon are shown in Fig. 8. The terms ‘‘fracture flow’’ and ‘‘matrix flow’’ are defined as mass flux of water flowing through fractures or matrix, respectively. Summation of fracture and matrix flows gives total flow or percolation flux.

Fig. 8(a) and (b) shows that fracture flow is predominant, as compared to matrix flow for the same climate scenario, at the level of the potential repository. Table 3 lists the percentage of fracture–matrix flow components at the potential repository horizon and the

water table as a percentage of the total flux. These statistics, predicted using the 18 simulation results of nine infiltration maps and two perched-water conceptual models, provide important input data for the system performance assessment. They show that fracture flow is dominant both at the potential repository horizon and at the water table in all 18 flow fields.

4.3. PTn flow studies

The PTn hydrogeological unit plays a potential significant role in assessing repository performance by altering the pattern of percolation into the underlying TSw unit. A key issue is whether the PTn is dominated by matrix flow, resulting in a generally uniform percolation flux into the underlying repository rocks of the TSw, or whether preferential flow paths within the PTn serve to focus flow above or around potential repository drifts. The PTn unit consists of non- to partially welded tuffs, and it extends from the base of the densely welded and devitrified portion of the Tiva Canyon Tuff to the top of the densely welded portion of the TSw. The combined thickness of these layers exceeds 150 m at the northern end of Yucca Mountain, while at the southern end, the PTn thins to less than 30 m.

The PTn unit displays significantly different hydrogeological characteristics from the TCw and TSw units that bound it. Both the TCw and the TSw are characterized by dense welding and intense fracturing. Where exposed at the land surface, the TCw plays an important role in controlling net surface infiltration, since fracturing through the low-porosity matrix may initiate rapid vertical percolation. During percolation through the PTn, the flow pattern changes from fracture-dominated flow in the TCw, to matrix-dominated flow within the PTn, to the initiation of significant fracture flow in the upper layers of the TSw. In the 3-D UZ flow model, the PTn unit is represented using six lateral model layers (Fig. 2). This may be very coarse for detailed analyses to capture flow effects for thin layers (<10 m) of the PTn.

The conceptual model for the current UZ flow studies at Yucca Mountain relies on a steady-state flow assumption. Net infiltration at the bedrock surface (top of the TCw unit) is actually episodic, with significant pulses probably occurring only once every few years. These spatially and temporally variable pulses of moisture percolate rapidly through the highly fractured tuffs of the TCw, as indicated by the numerous bomb-pulse chlorine-36 signatures measured within the TCw (Fabryka-Martin, 2000). However, at the TCw–PTn interface, where welded tuffs grade sharply into nonwelded tuffs, flow behavior changes from fracture-dominated to matrix-dominated flow. The highly porous PTn matrix may significantly attenuate the episodic infiltration flux; however, in localized areas such as around faults and zones with high infiltration rates, fracture flow within the PTn may still predominate. In general, the high storage capacity of the PTn matrix tends to damp moisture flow through the unit so that percolation flux across the bottom of the PTn into the TSw is more uniformly distributed spatially and temporally for the areas far away from faults. Therefore, the net episodic surface infiltration may be approximated as steady state for flow through the units below the PTn.

The flow pattern through the PTn unit can be analyzed using the modeling results. The simulations reveal two types of lateral flow diversion through the PTn: (1) up to a hundred

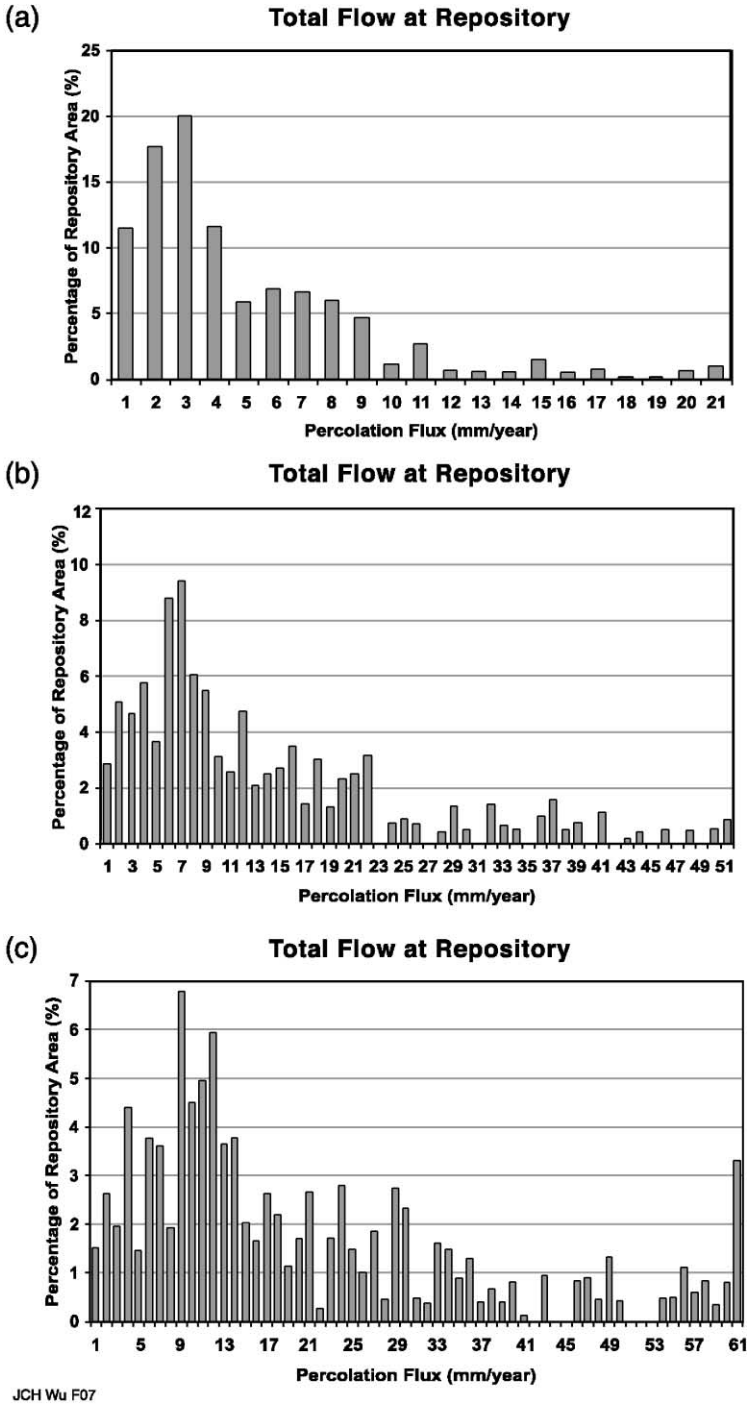
(a)
Total Flow at Repository
Percentage of Repository Area (%)
0 5 10 15 20 25
1 2 3 4 5 6 7 8 9 10 11 12 13 14 15 16 17 18 19 20 21
Percolation Flux (mm/year)
(b)
Total Flow at Repository
Percentage of Repository Area (%)
0 2 4 6 8 10 12
1 3 5 7 9 11 13 15 17 19 21 23 25 27 29 31 33 35 37 39 41 43 45 47 49 51
Percolation Flux (mm/year)
(c)
Total Flow at Repository
Percentage of Repository Area (%)
0 1 2 3 4 5 6 7
1 5 9 13 17 21 25 29 33 37 41 45 49 53 57 61
Percolation Flux (mm/year)
JCH Wu F07

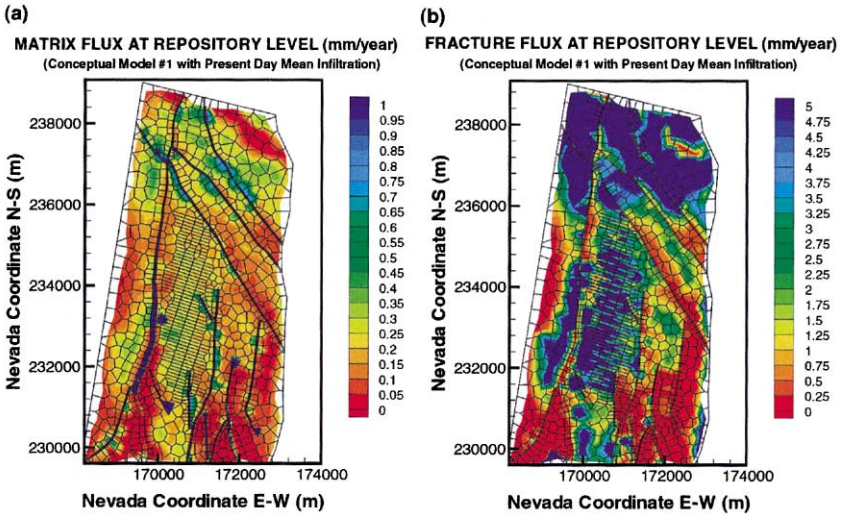

Fig. 8. Matrix flow (a) and fracture flow (b) at repository horizon, simulated using the present-day, mean infiltration rate.

meters movement to the east in the areas above the potential repository and (2) lateral diversion into major faults (e.g., Solitario Canyon and Ghost Dance). In general, high infiltration zones of the mountain crest along the middle, north–south model domain are damped and spread into larger areas after crossing the PTn.

Table 4 compares the fraction of vertical fracture–matrix flow at the middle of the PTn with that at the repository horizon below. Note that on the ground surface, infiltration is introduced into fractures only; therefore, it is 100% fracture flow at the top of model domain. The statistics in Table 4 shows that matrix flow is dominant in the PTn unit, taking nearly 90% of the total flow and with little variation among the three climate scenarios. This indicates that a dramatic transition takes place from fracture-dominant flow within the TCw down to matrix-dominant flow in the PTn, crossing the interface between the TCw and PTn units. While flowing continuously down across the PTn and TSw interface, percolation flux changes back from matrix-dominated to fracture matrix-dominated flow into the TSw, as indicated by the statistics in Table 4.

4.4. Effects of major faults

Major faults may provide a direct path from the repository horizon to the water table and thus significantly affect the ambient hydrogeologic system as well as flow and transport processes at Yucca Mountain. This is particularly significant for the strategy of waste isolation because radionuclides released from the potential repository could bypass altered,

Fig. 7. Areal frequency and distribution of simulated percolation fluxes within the repository horizon under three mean infiltration rates: (a) present day; (b) monsoon; and (c) glacial transition.

Table 3
Comparison of the water flux through fractures as a percentage of the total flux at two different horizons (1) at the potential repository and (2) at the water table, using the nine infiltration scenarios and two perched-water conceptual models

Climate		Present-day		Monsoon		Glacial transition	
Perched model	Infiltration	Potential repository (%)	Water table (%)	Potential repository (%)	Water table (%)	Potential repository (%)	Water table (%)
#1	low	86.6	84.7	90.0	90.1	86.9	87.2
#2	low	86.4	69.4	89.9	76.6	86.8	71.4
#1	mean	83.7	86.7	89.5	90.2	91.4	90.5
#2	mean	83.7	71.2	89.5	80.9	91.4	83.4
#1	upper	94.5	95.4	95.6	96.5	96.5	96.9
#2	upper	94.3	82.1	95.5	83.9	96.4	89.0

zeolitic or vitric layers within the CHn hydrogeologic unit, where they could be retarded by sorption. Alternatively, faults might be considered a positive feature of the site if they divert water around waste emplacement drifts or prevent laterally flowing water from focusing at the area of waste emplacement. Compared to the surrounding rock, larger fracture apertures and higher fracture densities generally lead to increased permeability and reduced capillarity within and near faults or fault zones. Flow is also affected by the amount of offset at the fault, which can range from meters to hundreds of meters. However, quantitative analyses of faults and their roles prove to be difficult because only limited tests have been performed on faults and there exist large uncertainties in fault properties.

Fig. 2 shows several vertical and inclined faults and fault displacements along the vertical cross section of the east–west UZ model domain. In this section, we investigate the conceptual model of fault influence on the hydrogeologic system using the UZ flow model, in which faults are represented using a vertical or inclined walls 30 m thick. Vertically, faults are subdivided into four hydrogeological units, according to their connections to the neighboring nonfaulting rocks, in the four major hydrogeological units of TCw, PTn, TSw, and CHn. Therefore, each fault, as shown in Fig. 2, is represented in the model as a vertical or inclined 3-D sheet of gridblocks. The rock properties of faults were estimated using a two-dimensional inversion of saturation, water potential, and pneumatic data (Ahlers and Liu, 2000).

An example of the effects of faults on UZ flow is presented in Fig. 9(a) and (b), using the simulation results from the present-day, mean infiltration map. A comparison of the

Table 4
Comparison of the water flux through matrix and fractures as a percentage of the total flux at the middle PTn and at the potential repository

Climate	Flux at middle PTn (%)		Flux at potential repository (%)	
	Fracture	Matrix	Fracture	Matrix
Present-day	11.6	88.4	83.7	16.3
Monsoon	12.1	87.9	89.5	10.5
Glacial transition	11.8	88.2	91.4	8.6

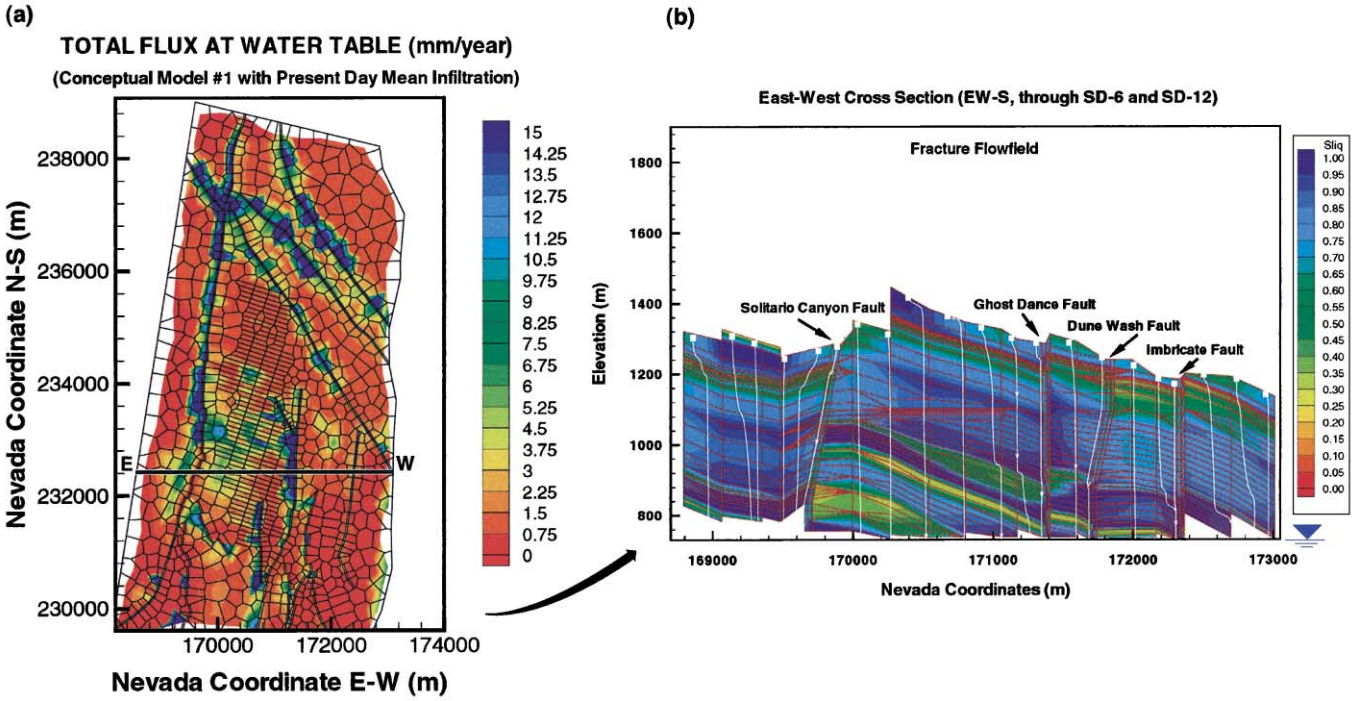

Fig. 9. Effects of faults on UZ flow for the present-day, mean infiltration rate; (a) simulated fluxes at the water table, (b) simulated groundwater flowpaths (white lines indicating flow lines releasing from the top boundary, red lines for connections of gridblock centers, and background colors showing matrix liquid saturation) along the west–east cross section within fracture–fracture flow fields.

Table 5
Comparison of the water flux through faults as a percentage of the total flux at four different horizons (1) on ground surface; (2) interface between PTn and TSw; (3) at the potential repository; and (4) at the water table

Climate scenarios; mean infiltration (mm/year)	Fraction of total flow through faults (%)											
	Ground surface			PTn–TSw interface			Potential repository level			Water table		
	Total	South	North	Total	South	North	Total	South	North	Total	South	North
Present-day; 4.6	3.8	3.6	3.9	14.3	18.9	12.7	14.6	19.8	12.7	34.9	15.9	42.0
Monsoon; 12.4	4.1	3.8	4.2	10.5	13.0	9.6	10.5	13.3	9.5	42.4	21.9	51.3
Glacial transition; 18.0	4.0	3.7	4.1	9.1	10.8	8.4	9.1	11.0	8.2	44.4	24.3	54.2

Total denotes flow over the entire model domain, South denotes flow over southern part/half model domain with north Nevada coordinate less than 233,500 m; and North denotes flow over northern part/half model domain.

flux pattern between surface infiltration (Fig. 3(b)) and the water table map (Fig. 9(a)) clearly indicates that under the current conceptual model of faults, flow has been significantly diverted to the faults while penetrating the UZ system. At the top boundary, infiltration rates or distributions, as shown in Fig. 3(b), are located independently of fault locations. However, upon arriving at the water table, a large fraction of the water has been diverted to the Solitaro Canyon, Ghost Dance, and other faults in the model domain.

The effects of faults on UZ flow under the current conceptual model can be analyzed using vertical flowpath plots. Fig. 9(b) displays such results, showing flow fields through fractures (flow through matrix is similar) along a west–east cross section. The flowpath results shown along the 2-D cross section are extracted from the 3-D flow fields and the background contours show liquid saturation in the matrix. Fig. 9(b) shows that flowpaths

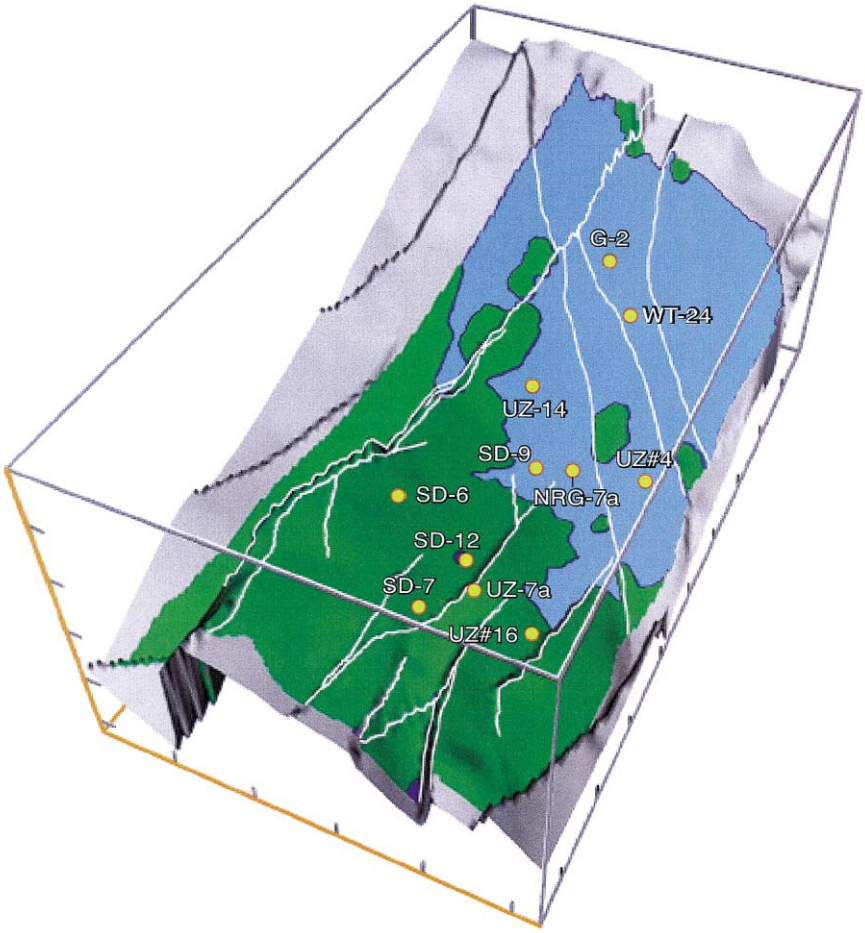

Fig. 10. Simulated 3-D view of perched-water bodies along the base of the TSw, using the simulation results of Conceptual Model #1 with present-day, mean infiltration rate (the blue contours denote the domain with 100% water saturation and the green for the areas with less than 100% water saturation).

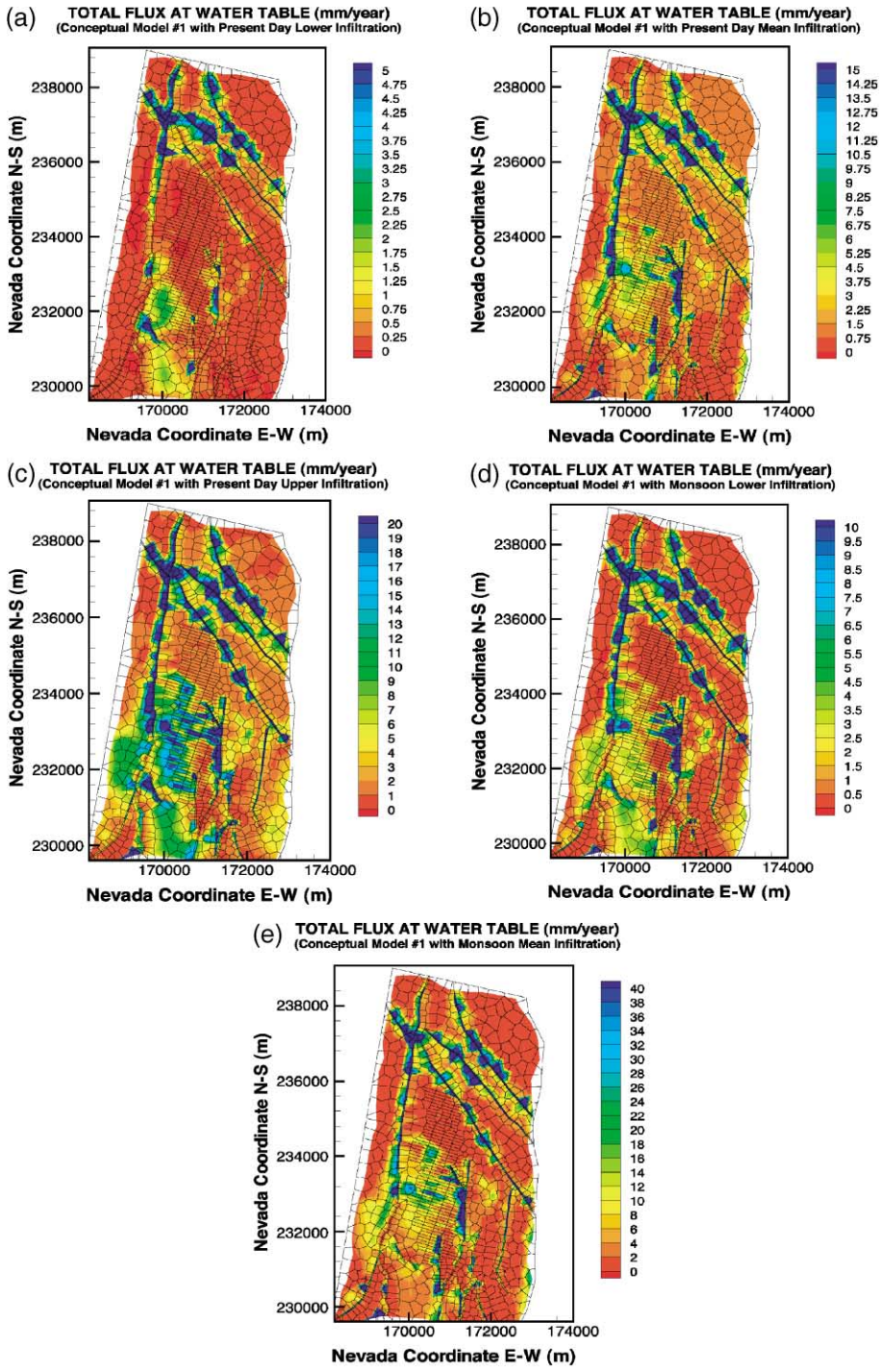
(a) TOTAL FLUX AT WATER TABLE (mm/year)
(Conceptual Model #1 with Present Day Lower Infiltration)
(b) TOTAL FLUX AT WATER TABLE (mm/year)
(Conceptual Model #1 with Present Day Mean Infiltration)
(c) TOTAL FLUX AT WATER TABLE (mm/year)
(Conceptual Model #1 with Present Day Upper Infiltration)
(d) TOTAL FLUX AT WATER TABLE (mm/year)
(Conceptual Model #1 with Monsoon Lower Infiltration)
(e) TOTAL FLUX AT WATER TABLE (mm/year)
(Conceptual Model #1 with Monsoon Mean Infiltration)
Nevada Coordinate N-S (m)
Nevada Coordinate E-W (m)
238000
236000
234000
232000
230000
170000
172000
174000

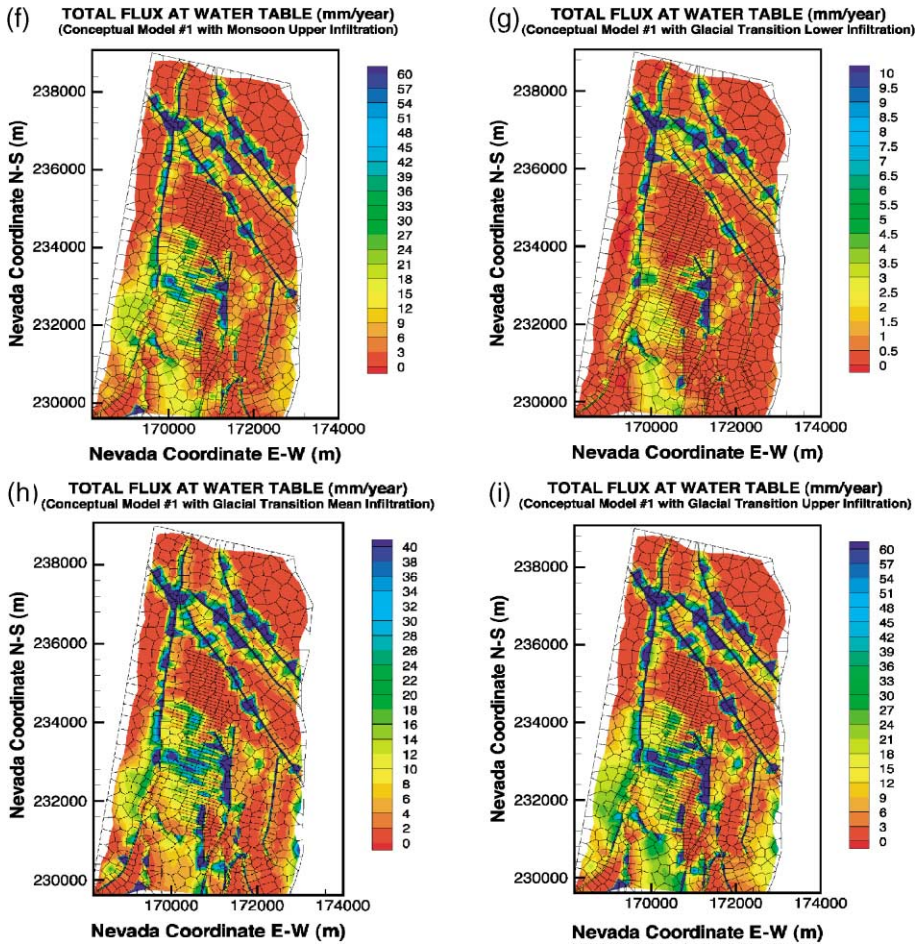

Fig. 11. Simulated fluxes at the water table using Conceptual Model #1 for the nine current and future climate scenarios: (a) present-day, lower-bound; (b) present-day, mean; (c) present-day, upper-bound; (d) monsoon, lower bound; (e) monsoon, mean; (f) monsoon, upper-bound; (g) glacial, lower-bound; (h) glacial, mean; and (i) glacial, upper-bound.

for particles released in the surface areas close to faults either converge down along or parallel to faults. No flow lines are seen to cross faults within the cross section. This indicates that faults can serve as either capillary barriers or downward flow conduits for UZ percolation.

Examination of the simulation results reveals that the fraction of flow occurring through the faults, as a percentage of the total flow (through the fractures, matrix, and faults), increases with depth. Table 5 lists these percentages at four different horizons for the three climate scenarios. At the ground surface, 4% of the total flow occurs through the faults. This percentage increases to 10–15% for flow through the PTn. At the water table, fault flow accounts for 35–44% of the total flow. The percentage of fault flow at the water table

is the most sensitive to the climate scenario compared to the other horizons. It increases from 35% to 42% to 44% going from present-day, to monsoon and to glacial-transition climates, respectively. In addition, Table 5 shows that flow percentages through faults at the water table in the southern part (through vitric zones) are very different from the northern part (through zeolitic zones) of the model domain. Fault flow consists of 42%, 51%, and 54% of the total flow in the northern model domain versus only 16%, 22%, and 24% in the south for the three infiltration scenarios. This indicates more lateral flow diversion occurring in the north when crossing the low-permeability zeolitic zones of the CHn.

4.5. Calico Hills unit and perched water

In terms of groundwater flowpaths and travel times, as well as radionuclide transport from the repository level to the saturated zone, the CHn hydrogeologic unit plays a crucial role. This unit separates the potential repository horizon from the saturated zone. The predominantly nonwelded nature of the CHn makes these initially high-porosity, vitric tuffs susceptible to hydrothermal alteration. Hydrothermal alteration produces low-permeability clays and zeolites that create complex, heterogeneous flow paths within the unit. The observed widespread alteration within the CHn has impacts for perched-water occurrence, for groundwater flow paths and travel times, and for radionuclide transport as well, because of the reduced permeability and the sorptive potential associated with zeolitic rocks.

Within the UZ flow model, the CHn is represented with 14 model layers based on lithostratigraphy and available hydrogeologic properties (Fig. 2). The CHn unit extends from the base of the lower welded vitrophyre of the TSw to the top of the welded portion of the Bullfrog Tuff. The CHn consists of the non- to partially welded vitric subzone of the lower TSw, the pre-Topopah Spring bedded tuffs, the Calico Hills Formation, the pre-Calico Hills bedded tuffs, the entire Prow Pass Tuff, and the upper nonwelded, vitric portions of the Bullfrog Tuff. The cumulative unsaturated thickness of the CHn ranges from about 400 m at the northern end of Yucca Mountain to approximately 200 m near the southern end.

Simulations using the two conceptual perched-water models (see Section 3) incorporate all the three climate scenarios (present-day, monsoon and glacial transition) and their associated lower-bound, mean, or upper-bound infiltration maps. Both perched-water conceptual models can generally match the water perching conditions, as observed in Yucca Mountain. Fig. 10 presents a simulated perspective view of 3-D perched-water bodies and their volumetric extensions. This figure shows water saturation distributions, in fractures, along the bottom of the TSw or the low basal vitrophyre layer with Conceptual Model #1. The blue isosurfaces on the figure reflect the regions near 100% liquid saturation or perched-water zones, within fractures along the model layer, while the green isosurface represents a portion of the model layer with fracture liquid saturations less than 100%. Fig. 10 clearly shows several extensive perched-water bodies, separated by faults, predicted to be present in the northern part of the model domain.

Effects of perched-water zones on flow processes in the CHn unit may be best explained by comparing percolation fluxes simulated at the repository level with those at the water table. Fig. 11(a)–(i) presents the simulated percolation fluxes at the water table for the nine mean infiltration rates of present-day, monsoon, and glacial-transition

climates with Conceptual Model #1. The simulated percolation fluxes for these nine climates at the repository level are shown on Fig. 6(a)–(i).

Figs. 6 and 11 show large differences in the magnitude and distribution of percolation fluxes and their distributions at the water table from their counterpart at the repository horizon. In addition, the simulation results confirm significant lateral flow or diversion occurring above or within the CHn from both perched-water models. Comparing the flux distribution in the northern part of the model domain indicates high percolation fluxes at the water table, which is focused along the major faults. Compared to the flow patterns at the repository level, the water table flux maps of Fig. 11 show significantly lower fluxes (red zone) in the northern part of the potential repository area, directly below the perched-water bodies and bounded by the Solitario Canyon and the Drillhole Wash faults. A large amount of water is diverted laterally to the east, along layer slopes, and intersects faults that focus flow downward to the water table.

In the southern part, below the potential repository area, the majority of percolation flux at the water table is found to be contributed by matrix flow in the high-permeability vitric zones. Even in these areas, however, certain amount of water is laterally diverted to the east and intercepted by faults along the thin zeolitic layers, as seen by comparing the repository fluxes with the water table fluxes.

5. Transport simulation results and analyses

This section summarizes our studies of tracer/radionuclide transport using the 21 3-D flow fields. The results present a comprehensive analysis of transport processes of radionuclides from the repository to the water table, including understandings on the effects of various climate or infiltration scenarios, different perched-water conceptual models, and adsorption onto rocks.

5.1. Modeling procedure and transport parameters

Simulation results and analyses of this work are based on transport studies of conservative and reactive tracers using a decoupled version of the T2R3D code (Wu and Pruess, 2000). These modeling studies are conducted to obtain insight into radionuclide transport from the repository to the water table. The dual-permeability modeling approach as well as the same 3-D grid (Figs. 1 and 2) are used in the transport simulations.

Table 6
K_d values used for a reactive tracer transport in different hydrogeologic units (Wu et al., 2000)

Hydrogeologic unit	K_d (cc/g)
Zeolitic matrix in CHn	4.0
Vitric matrix in CHn	1.0
Matrix in TSw	1.0
Fault matrix in CHn	1.0
Fractures and the matrix in the rest of units	0.0

The 21 steady-state, 3-D flow fields, as discussed in Section 4, are directly used as input to the T2R3D code for transport runs.

Tracers or radionuclides are treated as conservative (nonadsorbing) and reactive (adsorbing) components transported through the UZ. For both cases, the mechanical dispersion effect through the fracture–matrix system is ignored, because it was found to be insensitive to modeled results for the flow system considered. A constant molecular diffusion coefficient of 3.2×10^{-11} (m^2/s) is used for matrix diffusion of the conservative component, and 1.6×10^{-10} (m^2/s) is used for the reactive component. In the case of a reactive or adsorbing tracer, several K_d values are used for different units, as given in Table 6, and these values were selected to approximate those for neptunium (^{237}Np) transport property. All transport simulations were run to 1,000,000 years under steady-state flow fields with constant initial source concentration conditions at the repository fracture blocks. This is to assume that a tracer/radionuclide is released at the starting time of a simulation instantaneously from fractures of the repository.

5.2. Simulation scenarios

For each of the 21 flow simulations, we conducted two transport runs—one for conservative and the other for reactive tracer, respectively. Table 7 lists 7×2 modeling scenarios with the present-day, mean infiltration climates, out of a total of 21×2 simulation scenarios, associated with conceptual models and the corresponding three climates infiltration maps. In this table, the odd transport simulation numbers represent transport simulation for conservative/nonadsorbing tracer/radionuclide and the even simulation numbers represent reactive/adsorbing tracer/radionuclide transport.

5.3. Transport simulation results and analyses

Tracer transport times (since release from the repository to the water table) can be analyzed using a cumulative or fractional breakthrough curve, as shown in Fig. 12 for the present-day infiltration scenario. The fractional mass breakthrough in these figures is defined as the cumulative mass of tracer or radionuclide arriving at the water table over the entire bottom model boundary over time, normalized by the total initial mass of the component at the repository. In the figure, solid-line curves represent simulation results of

Table 7
Fourteen transport simulation scenarios for the present-day infiltration rates

Transport simulation	Perched-water conceptual model	Infiltration map
P-T#1 P-T#2	#3	present-day, mean infiltration
P-T#3 P-T#4	#1	present-day, lower-bound infiltration
P-T#5 P-T#6	#2	present-day, lower-bound infiltration
P-T#7 P-T#8	#1	present-day, mean infiltration
P-T#9 P-T#10	#2	present-day, mean infiltration
P-T#11 P-T#12	#1	present-day, upper-bound infiltration
P-T#13 P-T#14	#2	present-day, upper-bound infiltration

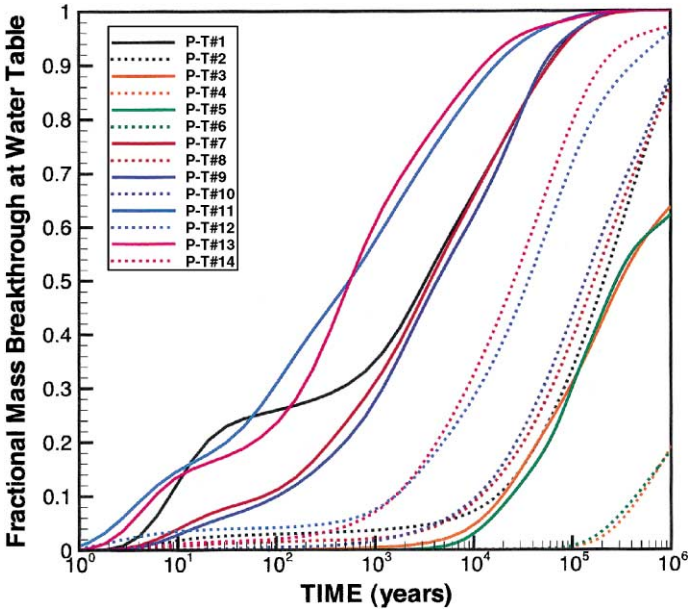

Fig. 12. Simulated breakthrough curves of cumulative tracer/radionuclide mass arriving at the water table, after release from the repository, using the three present-day infiltration scenarios and three conceptual models.

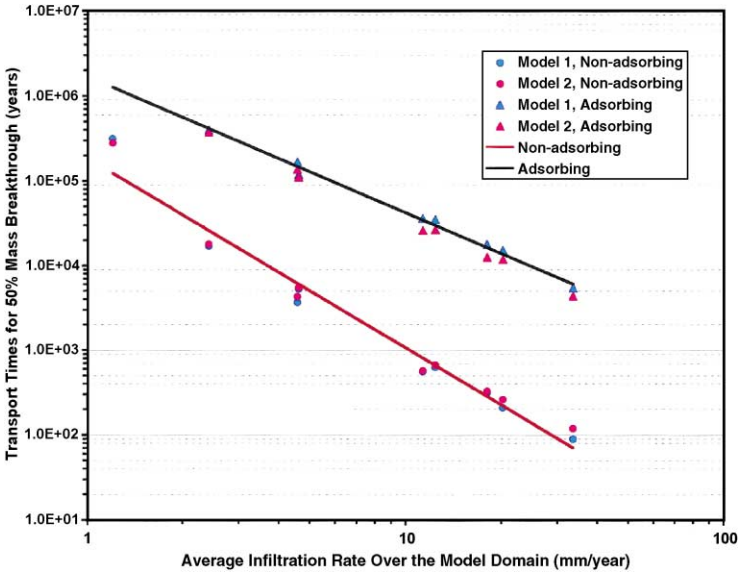

Fig. 13. Correlations of average infiltration rates and tracer transport times at 50% mass breakthrough for the 42 simulation scenarios.

conservative/nonadsorbing tracer transport, and dotted-line plots are for reactive, adsorbing tracer transport. The 42 transport simulations (e.g., Fig. 12) show a wide range of tracer/radionuclide transport times with different climates, type of tracers, and perched-water conceptual models. The predominant factors in tracer transport times, as indicated by these modeling results, are (1) surface-infiltration rates or climate scenarios (2) sorption effects, whether the tracer is conservative or reactive. To a certain extent, perched-water conceptual models also affect tracer transport times significantly. However, the overall impact of the perched-water conceptual models on tracer breakthrough at the water table are found to be secondary compared with the effects of infiltration and adsorption.

Fig. 13 correlates average infiltration rates and tracer transport times at 50% mass breakthrough (or mean) for the 42 simulation scenarios, including all the nine climatic scenarios, the two perched-water conceptual models and the nonperched-water model. Fig. 13 shows that the average tracer transport times are inversely proportional to the average surface infiltration (net water recharge) rate over the model domain. As the net infiltration rate increases from 5 to 35 (mm/year), averaged tracer transport (50% breakthrough) times decrease by two to three orders of magnitude. As infiltration rates increase, adsorbing tracer has a lower decreasing rate of transport time than a nonadsorbing tracer reflecting retardation effects in the matrix system. Without accounting for adsorption onto matrix rocks, as shown in Fig. 13, nonadsorbing tracers migrate much faster than adsorbing ones. There is a two-orders-of-magnitude difference in travel times for the two types of tracers under the same infiltration conditions.

6. Summary and conclusions

A large-scale modeling study is presented for characterizing fluid flow and tracer/radionuclide transport in the UZ of Yucca Mountain potential repository. The methodology used in the characterization studies includes (1) design of a proper 3-D grid that incorporates complicated geological features, including 3-D, inclined faults, (2) model calibrations against field data, and (3) flow and transport simulation studies using different climate scenarios and hydrogeological conceptual models.

Using different climate scenarios and conceptual models, the simulated flow fields predict percolation distribution within the UZ system, components of fracture and matrix flow, probable flow paths below the potential repository, and groundwater travel times. The modeled percolation fluxes and their distributions show that fracture flow is predicted to be dominant in the welded tuff, both at the potential repository horizon and at the water table. The model results also indicate that percolation flux at the middle of the PTn is predominantly matrix flow, comprising nearly 90% of the total flow. On the other hand, all the flow modeling scenarios indicate significant lateral flow diversion occurring at the CHn resulting due to the presence of perched water or thick low-permeability zeolitic layers. Faults act as major flow paths through the CHn under the current conceptualization. The percentage of fault flow versus total percolation fluxes increases as mean infiltration rates increase with depth.

Tracer-transport studies indicate that there exists a wide range of tracer transport times associated with different climate scenarios, types of tracers/radionuclides, and perched-

water conceptual models. Sensitivity analyses identify that surface infiltration rates and adsorption effects in the CHn unit are the most important factors for determining tracer immigration from the repository to the water table.

The flow and transport characterization of this work constitutes an important step in understanding fluid flow and radionuclide transport processes at Yucca Mountain. However, there are still considerable limitations and uncertainties with the current model and its results. In particular, uncertainties associated with the 3-D flow fields are largely attributed to the limited data available to characterize the spatial and temporal distribution of net infiltration or future climates as well as the spatial variability of rock hydrologic properties. This also imparts uncertainty in conceptual models used to describe flow behavior, since these models are developed primarily from site data. The assumption of steady-state flow and the use of layer-averaged rock parameters are among these conceptual uncertainties. In addition, the dual-continuum modeling approach used employs large-scale spatial and temporal averaging in representing the heterogeneous fracture and matrix system. This volume-averaged concept may fail to capture phenomena associated with "focusing" flow and transport along localized preferential pathways along large, well-connected fractures (other than faults) or on a much smaller scale than grid block size. Even though it is possible to simulate those localized flow and transport processes using a volume averaged, continuum approach with sufficiently detailed grid resolution, the lack in detailed knowledge of fracture/matrix properties and their spatial distributions currently prevents such a modeling effort.

Through bounding and sensitivity studies, as demonstrated in this work, uncertainties in the 3-D flow fields can be identified, constrained, and perhaps quantified. For example, a systematic sensitivity analysis using a large number of numerical simulations of this work may provide important data to examine the effects of current and future climate scenarios on UZ flow. This helps bound model predictions of system responses during potential future climatic conditions. Different conceptual models, in particular those related to perched water below the potential repository horizon, have been developed and modeled to assess the sensitivity of model results to changes in model parameters.

Overall, the simulated flow-field and tracer-transport results show greatest sensitivity to the distribution and magnitude of net infiltration. Assumptions regarding the conceptualization and parameterization of fractures within the CHn unit and of fault zones have large uncertainties (as a result of limited data), yet these UZ features appear to have a significant impact on flow behavior below the repository. Additional sensitivity studies, using different conceptual models and a range of hydrologic parameters for fractures and faults, are needed to assess the potential range of variability in flow behavior between the repository horizon and the water table.

Acknowledgements

We would like to thank Andre Unger and Dan Hawkes for their review of this paper. We would also like to thank the two anonymous reviewers and Prof. E.O. Frind for their insightful and constructive comments and suggestions to improve the manuscript. In addition, we are grateful to Diana Swantek and Jennifer Hinds for their assistance in

plotting the figures. This work was supported by the Director, Office of Civilian Radioactive Waste Management, US Department of Energy, through Memorandum Purchase Order EA9013MC5X between TRW Environmental Safety Systems and the Ernest Orlando Lawrence Berkeley National Laboratory. The support is provided to Lawrence Berkeley National Laboratory through the US Department of Energy contract no. DE-AC03-76SF00098.

References

Ahlers, C.F., Liu, H.H., 2000. Calibrated Properties Model. Report MDL-NBS-HS-000003. Berkeley, California: Lawrence Berkeley Laboratory. Las Vegas, Nevada: CRWMS M and O.

Ahlers, C.F., Bandurraga, T.M., Bodvarsson, G.S., Chen, G., Finsterle, S., Wu, Y.S., 1995. Performance Analysis of the LBNL/USGS Three-Dimensional Unsaturated Zone Site-Scale Model, Yucca Mountain Project Milestone 3GLM105M. Lawrence Berkeley National Laboratory, Berkeley, CA.

Buesch, D.C., Spengler, R.W., Nelson, P.H., Vaniman, D.T., Chipera, S.J., Bish, D.L., 1995. Geometry of the Vitric–Zeolitic Transition in Tuffs and the Relation to Fault Zones at Yucca Mountain, Nevada. International Union of Geodesy and Geophysics, Boulder, Colorado, XXI General Assembly, July 2–14, p. A426.

Day, W.C., Potter, C.J., Sweetkind, D.E., Dickerson, R.P., San Juan, C.A., 1998. Bedrock Geologic Map of the Central Block Area, Yucca Mountain, Nye County, Nevada. Map I-2601. US Geological Survey, Washington, DC.

Fabryka-Martin, J.T., 2000. Analysis of Geochemical Data for the Unsaturated Zone. Report ANL-NBS-GS-00004. Los Alamos, NM: Los Alamos National Laboratory/ Washington, DC: US Geological Survey. Las Vegas, Nevada: CRWMS M and O.

Flint, A.L., Hevesi, J.A., Flint, E.L., 1996. Conceptual and Numerical Model of infiltration for the Yucca Mountain Area, Nevada, US Geological Survey, Water-Resources Investigation Report-96, Denver, Colorado.

Forrester, R., 2000. Future Climate Analysis. Report ANL-NBS-HS-000032. US Geological Survey, Denver, Colorado.

Hevesi, J., Flint, L., 2000. Simulation of Net Infiltration for Modern and Potential Future Climate. Report ANL-NBS-GS-000008. US Geological Survey, Denver, Colorado.

Liu, H.H., 2000. Analysis of Hydrologic Properties. Report ANL-NBS-HS-000002. Berkeley, California: Lawrence Berkeley Laboratory. Las Vegas, Nevada: CRWMS M and O.

Liu, H.H., Doughty, C., Bodvarsson, G.S., 1998. An active fracture model for unsaturated flow and transport in fractured rocks. Water Resour. Res. 34, 2633–2646.

McLaren, R.G., Forsyth, P.A., Sudicky, E.A., VanderKwaak, J.E., Schwartz, F.W., Kessler, J.H., 2000. Flow and transport in fractured tuff at Yucca Mountain: numerical experiments on fast preferential flow mechanisms. J. Contam. Hydrol. 43, 211–238.

Montazer, P., Wilson, W.E., 1984. Conceptual Hydrologic Model of Flow in the Unsaturated Zone, Yucca Mountain, Nevada. Water-Resources Investigations Report 84-4345. US Geological Survey, Lakewood, Colorado.

Pan, L., Hinds, J., Haukwa, C., Wu, Y.S., Bodvarsson, G.S., 2000. WinGrider: An Interactive Grid Generator for TOUGH2, Version 1.0 (Users' Manual). Earth Sciences Division, Lawrence Berkeley National Laboratory, Berkeley California.

Pollock, D.W., 1986. Simulation of fluid flow and energy transport processes associated with high-level radioactive waste disposal in unsaturated alluvium. Water Resour. Res. 22 (5), 765–775.

Pruess, K., 1991. TOUGH2-A General-Purpose Numerical Simulator for Multiphase Fluid and Heat Flow. LBL-29400. Lawrence Berkeley Laboratory, Berkeley, California.

Robinson, B.A., Wolfsberg, A.V., Viswanathan, H.S., Gable, C.W., Zyvoloski, G.A., Turin, H.J., 1996. Modeling of Flow Radionuclide Migration and Environmental Isotope Distributions at Yucca Mountain. Sandia National Laboratories, Milestone 3672, Albuquerque, New Mexico.

Rousseau, J.P., Kwicklis, E.M., Gillies, C. (Eds.), 1998. Hydrogeology of the unsaturated zone, North Ramp area

of the Exploratory Studies Facility, Yucca Mountain, Nevada, US Geological Survey, Water-Resources Investigations 98-4050.

Rulon, J., Bodvarsson, G.S., Montazer, P., 1986. Preliminary Numerical Simulations of Groundwater Flow in the Unsaturated Zone, Yucca Mountain, Nevada. LBL-20553. Lawrence Berkeley Laboratory, Berkeley, California.

Scott, R.B., Bonk, J., 1984. Preliminary Geologic Map of Yucca Mountain, Nye County, Nevada, with Geologic Sections. Open-File Report 84-494. US Geological Survey, Denver, Colorado.

Tsang, Y.W., Pruess, K., 1987. A study of thermally induced convection near a high-level nuclear waste repository in partially saturated fracture tuff. Water Resour. Res. 23 (10), 1958–1966.

van Genuchten, M.Th., 1980. A closed-form equation for predicting the hydraulic conductivity of unsaturated soils. Soil Sci. Soc. Am. J. 44 (5), 892–898.

Viswanathan, H.S., Robinson, B.A., Valocchi, A.J., Triay, I.R., 1998. A reactive transport model of neptunium migration from the potential repository at Yucca Mountain. J. Hydrol. 209, 251–280.

Warren, J.E., Root, P.J., 1963. The behavior of naturally fractured reservoirs. Soc. Pet. Eng., J., Trans., AIME 228, 245–255.

Wittwer, C., Chen, G., Bodvarsson, G.S., Chornack, M., Flint, A., Flint, L., Kwicklis, E., Spengler, R., 1995. Preliminary Development of the LBL/USGS Three-Dimensional Site-Scale Model of Yucca Mountain, Nevada. LBL-37356. Lawrence Berkeley Laboratory, Berkeley, California.

Wu, Y.S., Pruess, K., 2000. Numerical simulation of non-isothermal multiphase tracer transport in heterogeneous fractured porous media. Adv. Water Resour. 23, 699–723.

Wu, Y.S., Ahlers, C.F., Fraser, P., Simmons, A., Pruess, K., 1996. Software Qualification Of Selected TOUGH2 Modules, Report LBL-39490; UC-800, Lawrence Berkeley National Laboratory, Berkeley, CA.

Wu, Y.S., Haukwa, C., Bodvarsson, G.S., 1999a. A site-scale model for fluid and heat flow in the unsaturated zone of Yucca Mountain, Nevada. J. Contam. Hydrol. 38 (1–3), 185–217.

Wu, Y.S., Ritcey, A.C., Bodvarsson, G.S., 1999b. A modeling study of perched water phenomena in the unsaturated zone at Yucca Mountain. J. Contam. Hydrol. 38 (1–3), 157–184.

Wu, Y.S., Liu, J., Xu, T., Haukwa, C., Zhang, W., Liu, H.H., Ahlers, C.F., 2000. UZ Flow Models and Submodels, Report MDL-NBS-HS-000006, Berkeley, California: Lawrence Berkeley National Laboratory. Las Vegas, Nevada, CRWMS M and O.